Proceedings of the 17th World Congress
The International Federation of Automatic Control
Seoul, Korea, July 6-11, 2008

Passive Robust Fault Detection using Interval MA Parity Equations: Inverse vs Direct Image Tests

Pedro Guerra * **Vicenç Puig** *

* *Automatic Control Department, Universitat Politècnica de Catalunya*
Rambla de Sant Nebridi, 11, 08222 Terrassa, Spain
(e-mail: vicenc.puig@upc.edu)

Abstract: In this paper, a passive robust fault detection test based on calculating the inverse image of an interval model (linear or non-linear but linear with respect to the parameters) expressed in MA form is presented. This relies on a consistency test which uses tools from interval analysis and zonotope arithmetic to check if there exists a member in the family of models described by an interval model that can explain the measured data. The proposed test is compared to the classical robust interval model fault detection approach based on the direct image. The main features of both tests will be extracted and advantages and drawbacks discussed using a motivational example. Finally, an application example based on the known quadruple-tank process is used to assess how the algorithms work.

Keywords: Fault detection, parity equations, zonotopes, robustness, uncertainty.

1. INTRODUCTION

Model-based fault detection methods rely on the concept of *analytical redundancy*. The simplest analytical redundancy schema consists on comparing measurements of a system with corresponding analytically computed values that in turn are computed from measurements of other variables and/or from previous measurements of the same variable. The resulting differences are called *residuals* and are assumed to be indicative of faults in the system. Under ideal conditions, residuals are zero in the absence of faults and non-zero when a fault is present. When the residual becomes non-zero the relations used to calculate the residual are considered to be invalid. However, modelling errors and disturbances in complex engineering systems are inevitable, leading the residuals to non-zero values even in the absence of faults. Thus, the residual generation stage is followed by a decision-making stage. A robust fault detection system invalidates a residual relation only if model uncertainty and/or disturbances can not explain the observed data, see Chen and Patton (1999). Approaches to robust fault detection are divided in two principal groups. In the first, often referred to as *active* robust fault detection, robustness is achieved by generating residuals from which the effect of model errors and disturbances have been decoupled. This leads to residuals which are insensitive to uncertainty and disturbances but at the same time sensitive to faults. This approach has been extensively developed the last years (see Chen and Patton (1999)). The main drawback of this approach is the need of decoupling, being not always possible. In the second approach, referred to as *passive*, the aim is to enhance the robustness of the fault detection system at the decision-making stage, mainly by using an adaptive threshold. A common approach to this problem is to inflate the allowable interval for the residual, or alternatively, for the model output prediction. so that false alarms due to model uncertainty are avoided. A limitation of this approach is that faults that produce a residual deviation smaller than the residual uncertainty due to model uncertainty will be missed.

A manner to represent model uncertainty is to bound parameter values on intervals. The resulting models are called *interval models* and have received a lot of attention in the context of robust fault detection, see among others Armengol et al. (2001); Puig et al. (2002); Fagarasan et al. (2004); Ploix and Adrot (2006). Generally in these publications the uncertainty interval for residuals (or predicted outputs) is computed by propagating the effect of the parameter uncertainty using a *direct image* of an interval function. This approach will be referred to as a *direct image test* in what follows. The residual relation is invalidated if the variable for which the interval is calculated leaves the interval.

In this paper a passive robust method will be presented where the *inverse image* of an interval model (linear or non-linear but linear with respect to the parameters) expressed in MA form is used to check wether there exists a member in the family of models, described by an interval model, that can explain the measured data. This inverse image test has already been suggested in Puig et al. (2006); Adrot and Ploix (2006) using subpavings and SIVIA algorithm (see Jaulin et al. (2001)). However, such implementation is computationally expensive and it can be made very efficient using zonotope representation. This test will be compared with the existing direct image test and the principal properties of the two tests extracted. These properties will be demonstrated by using an example.

The paper is organized in the following manner: Section 2 is dedicated to introducing the problem. In Sections 3 and 4, the earlier direct image test and the inverse image test are described for comparison. In Section 5 zonotopes and the related operations required for implementing fault detection tests are presented. An application example is presented in Section 6 to demonstrate how the algorithms work. Finally in Section 7 conclusions are drawn.

2. PROBLEM SET-UP

Let us consider that the output of the monitored system can be described by a (linear or non-linear but linear with respect to the parameters) MA model that can be expressed in regressor form as

$$y(k) = \varphi^T(k)\theta(k) + e(k) \tag{1}$$

$$\theta(k+1) = \theta(k) + w(k) \tag{2}$$

$$\theta(k) \in \Theta \tag{3}$$

where $\theta(k) \in \mathbb{R}^n$ is the parameter vector whose values are assumed to be unknown but to belong to a compact bounded initial set Θ, $\varphi(k) \in \mathbb{R}^n$ is the regressor vector which can contain any function of inputs and outputs, the noise and parameter variations terms are limited as

$$|e(k)| \leq \sigma \quad \text{and} \quad |w(k)| \leq \lambda \tag{4}$$

respectively. As the parameter vector is assumed to belong to $\mathbb{R}^n$ so does λ and the last inequality is an element wise inequality. Notice that this system description includes any system linear in the parameters. Parameter uncertainty comes from physical modelling or from the set-membership parameter estimation algorithms applied in a non-faulty situation.

Notice that Eq. (2) specifies the allowed temporal variation of uncertain parameters θ. Depending on the value of λ, three different cases can be considered:

- Time invariant case, $\lambda = 0$
- Time-varying case 1, $\lambda = \bar{\lambda}$
- Time-varying case 2, $\lambda = \infty$

In the first case, the parameter is unknown within Θ but it is known that it will not vary. In the second case, the parameter variation is bounded specifically by a vector $\bar{\lambda}$ while in the last case, the variation is implicitly bounded only by the initial parameter set Θ and can vary at will within that set.

The first case could represent situations when an initial variance comes from components specifications that are known only with a mean and variance in the beginning of the fault detection. The second case could represent a system that has been identified over a number of operation conditions, each with a different θ within Θ, but with the variance between samples bounded by $\bar{\lambda}$.

It is assumed that measurement data is available for N ($\geq n$) points, that is, series

$$\Phi_N = \{\varphi(k)\}_{k=0,\ldots,N-1} \qquad Y_N = \{y(k)\}_{k=0,\ldots,N-1} \tag{5}$$

are available at every time instant k.

Measurement noise can be taken into account by assuming that the measurements are known to belong to intervals $[y(k)]$, often created by adding an noise term $e(k)$ to the actual measurement $y(k)$, that is, $[y(k)] = [y(k) - e(k), y(k) + e(k)]$. The corresponding interval vector is

$$[Y_N(k)] = [y(k)] \times \cdots \times [y(k-N)] \subset \mathbb{R}^N$$

3. PASSIVE ROBUST FAULT DETECTION USING A DIRECT IMAGE TEST

As already noted in the introduction, fault detection using interval models has predominantly been based on calculating the *direct image* of functions related to trajectory generation in order to obtain the set which $\hat{y}(k)$ belongs to

$$\hat{\mathbb{Y}}(k) = \{\hat{y}(k) \mid \hat{y}(k) = \varphi^T(k)\theta(k), \theta(k) \in \Theta\} \tag{6}$$

In fault detection using the *direct image test*, the model is assumed invalidated and fault is indicated if $Y_N(k) \notin \hat{\mathbb{Y}}_N$ or, in the case of measurement noise, if

$$[Y_N(k)] \cap \hat{\mathbb{Y}}_N = \emptyset \tag{7}$$

As the evaluation of the image in Eq. (7) is complex even in the linear case, approximate envelopes are often used based on computing the interval hull of $\hat{\mathbb{Y}}$, denoted as $\square\hat{\mathbb{Y}}$. Envelopes are characterized as *sound* and *complete* according to how well they approximate $\square\hat{\mathbb{Y}}$. A sound envelope does not contain any region through which a trajectory does not cross, that is the envelope $[\hat{Y}]$ fulfills $[\hat{Y}] \subseteq \square\hat{\mathbb{Y}}$. A complete envelope $[\hat{Y}]$ on the other hand fulfills $\square\hat{\mathbb{Y}} \subseteq [\hat{Y}]$.

A general form of the fault detection algorithm using the direct image test is the following:

Algorithm 1 Fault detection using the direct image test

1: $fault \leftarrow FALSE$
2: $k \leftarrow 1$
3: **while** fault=FALSE **do**
4: Obtain input-output data $\{u(k), y(k)\}$ at time instant k and build regressor $\varphi(k)$.
5: Calculate $\hat{\mathbb{Y}}(k)$ as a direct image of Θ according to Eq. (6)
6: **if** $\hat{\mathbb{Y}}(k) \cap [y(k)] = \emptyset$
7: $fault \leftarrow TRUE$
8: **endif**
9: $k \leftarrow k + 1$
10: **end while**

It is known that it could be difficult to detect some faulty trajectories with the direct image test even when the envelope is sound and complete Armengol et al. (2001). This is due to the fact that many combinations of parameters can explain a set of data, a jump between these combinations will not be detected. On the other hand, using the direct image test it is difficult to consider explicitly the parameter variations presented in Eq. (4).

4. PASSIVE ROBUST FAULT DETECTION USING A INVERSE IMAGE TEST

4.1 Intuitive idea

An alternative fault detection test to check the consistency of the model given by Eqs. (1)-(3) will now be proposed which is based on the inverse image of the function in Eq. (1). Assume the measurement data $y(k)$ is available. Then, the interval $[y(k)]$ created by taking into account measurement noise $e(k)$. Intuitively, what is proposed now is a test based on computing the *inverse image* of $[y(k)]$, i.e.,

$$\hat{\Theta}(k) = f^{-1}[y(k)] \tag{8}$$

where $\hat{\Theta}(k)$ is the set of parameters consistent with the measurement data at time instant k. In this case, the model or parameter set Θ is invalidated if

$$\Theta \cap \hat{\Theta}(k) = \emptyset \tag{9}$$

A failed test means that there does not exist a $\theta \in \Theta$ that is consistent with the measurements.

4.2 Formalized idea

In order to formalize the inverse image test, the following definitions are introduced.

Definition 1. Let us consider the model description given by Eq. (1), for given data sequences Φ_N and Y_N introduced in 5, the parameter θ is said to belong to the *Feasible Solution Set* at time N, (denoted FSS_N), if there exist $\theta(0), \theta(2), \ldots, \theta(N-1)$ such that:

$$|y(k) - \varphi^T(k)\theta(k)| \leq \sigma \quad k = 0, \ldots, N-1 \tag{10}$$

$$|\theta(k) - \theta(k-1)| \leq \lambda \quad k = 1, \ldots, N-1 \tag{11}$$

$$\theta(0) \in \Theta \tag{12}$$

Using previous definition, a fault is now defined for the sequences Φ_N and Y_N.

Definition 2. For given data sequences Φ_N and Y_N, a *fault* is said to have occurred if the set FSS_N is empty.

Each new measurement defines a set of consistent parameters defined by

$$F_k = \{\theta \in \mathbb{R}^n : -\sigma \leq y(k) - \varphi(k)^T\theta \leq \sigma\} \tag{13}$$

F_k is the region between two hyperplanes. The normalized form of this strip is written as

$$\begin{aligned} F_k &= \{\theta \in \mathbb{R}^n : |\frac{y(k)}{\sigma} - \frac{\varphi(k)}{\sigma}^T \theta| \leq 1\} \\ &= \{\theta \in \mathbb{R}^n : |d(k) - c(k)^T\theta| \leq 1\} \end{aligned} \tag{14}$$

This strip F_k available at time k allows to iteratively detect the presence of a fault if its intersection with the feasible parameter set FSS_k is empty.

In practice, the computation of FSS_N is difficult. The fault detection algorithm presented in this paper is based on the use of zonotopes as an approximated feasible solution set, AFSS_N, that fulfills $\mathrm{FSS}_N \subseteq \mathrm{AFSS}_N$ for which consistency is checked. In the case when $\lambda > 0$, the set AFSS_N is expanded to take the allowed parameter variance into account in the next sample. The expanded set is denoted $\overline{\mathrm{AFSS}}_{N+1}$.

Algoritm 2 presents a general form of the suggested fault detection approach.

Algorithm 2 Fault detection using the inverse image test

1: $fault \leftarrow FALSE$
2: $k \leftarrow 1$
3: $\overline{AFSS}_k \leftarrow \Theta$
4: **while** fault=FALSE **do**
5: Obtain input-output data $\{u(k), y(k)\}$ at time instant k, build regressor $\varphi(k)$ and strip F_k according to Eq. (14).
6: **if** $\overline{AFSS}_k \cap F_k = \emptyset$
7: $fault \leftarrow TRUE$
8: **else** Calculate AFSS_k that fulfills $F_k \cap \overline{\mathrm{AFSS}}_k \subset \mathrm{AFSS}_k$ and
9: Expand AFSS_k taking into account λ to obtain $\overline{\mathrm{AFSS}}_{k+1}$.
10: **endif**
11: $k \leftarrow k + 1$
12: **end while**

5. ZONOTOPES AND RELATED OPERATIONS

5.1 Zonotopes

In this section, zonotopes and related operations will be presented as a tool to implement *Algorithm 1* and *Algorithm 2*.

Definition 3. The **Minkowski sum** of two sets $\mathbb{X}$ and $\mathbb{Y}$ is defined by $\mathbb{X} \oplus \mathbb{Y} = x + y : x \in \mathbb{X}, y \in \mathbb{Y}\}$.

Definition 4. Given a vector p $\in \mathbb{R}^n$ and a matrix H $\in \mathbb{R}^{n \times m}$, the Minkowski sum of the segments defined by the columns of matrix H, is called a **zonotope** of order m and it is represented as:

$$\mathbb{X} = p \oplus HB^m = \{p + Hz : z \in B^m\}$$

where: B^m is a unitary box, composed of m unitary intervals. The order m is a measure for the geometrical complexity of the zonotopes.

Looking at *Algorithm 1*, the required zonotope-based operations are: the direct image of a zonotope through a linear transformation (step 5) and the intersection between zonotopes (step 6). In case of *Algorithm 2*, the following zonotope-based operations are required: checking the consistency of a zonotope with a strip (step 6), intersection between a zonotope and a strip (step 8) and the expansion of the parameter set taking into account λ (step 9).

5.2 Image of a zonotope through a linear transformation

Consider a zonotope represented by $\mathbb{X} = p \oplus HB^m$ where $p \in \mathbb{R}^n$ is a vector and $H \in \mathbb{R}^{n \times m}$ is a matrix. The image of a zonotope through a linear transformation $M \in \mathbb{R}^{n \times n}$ is a zonotope $\mathbb{Y}$ defined by:

$$\mathbb{Y} = q \oplus NB^m \tag{15}$$

where: $q = Mp$ and $N = MH$.

5.3 Intersection between two zonotopes

Given two zonotopes $\mathbb{X}_1 = p_1 \oplus H_1 B^{r_1}$ and $\mathbb{X}_2 = p_2 \oplus H_2 B^{r_2}$ and matrix E, let us define:

$$\widehat{p}(E) = Ep_1 + (I - E)p_2 \tag{16}$$
$$\widehat{H}(E) = [EH_1 \;\; (I - E)H_2] \tag{17}$$

then,

$$\mathbb{X}_1 \cap \mathbb{X}_2 \subseteq \widehat{\mathbb{X}}(E) \tag{18}$$
$$\widehat{\mathbb{X}}(E) = \widehat{p}(E) \oplus \widehat{H}(E) B^{r_1 + r_2} \tag{19}$$

To reduce the size of the intersection zonotope $\widehat{\mathbb{X}}(E)$, a convex optimization problem is solved. If H_{1i} and H_{2j} (with i=1,$\cdots$,m_1, j=1,$\cdots$,m_2) are the columns of matrices H_1 and H_2, the function to be minimized is:

$$f(E) = \sum_{i=1}^{m_1} (EH_{1i})^T (EH_{1i}) + \sum_{j=1}^{m_2} (H_{2j} - EH_{2j})^T (H_{2j} - EH_{2j}) \tag{20}$$

5.4 Checking consistency of a zonotope with a strip

Given the zonotope $\mathbb{X} = p \oplus HB^r$, the strip $F = \{\theta \in \mathbb{R}^n : |c^T(k)\theta - d(k)| \leq \sigma\}$ and vector $\alpha \in \mathbb{R}^n$, we have:

$$\mathbb{X} \cap F \subseteq \Theta = \widehat{p}(\alpha) \oplus \widehat{H}(\alpha) B^{r+1} \tag{21}$$

where:

$$\widehat{p}(\alpha) = p + \alpha(d - c^T p) \tag{22}$$
$$\widehat{H}(\alpha) = [(I - \alpha c^T)H \;\; \sigma] \tag{23}$$

It is possible to choose the parameter vector α in such a way that a size criterion for the obtained bound is minimized. Here we use the method based in the Frobenius norm proposed in Alamo et al. (2005).

Given a new data point $\{y(k)\}$ at time instant k, regressor $\varphi(k)$ and strip F_k according to Eq. (14) are build. Assuming that $FSS_k \subseteq \mathbb{X}$ where $\mathbb{X} = p \oplus HB^m$ is a zonotope, consistency can be assessed by checking if

$$\mathbb{X} \cap F_k = \emptyset \tag{24}$$

This check is very easy to perform using the following definition:

Definition 5. A hyperplane $\mathbb{S} = \{x : c^T x = q\}$ is a **supporting hyperplane** of a zonotope $\mathbb{X} = p \oplus HB^m$ if either $c^T x \leq q_u, \forall x \in \mathbb{X}$ or else $c^T x \geq q_d, \forall x \in \mathbb{X}$ with equality occurring for some $x \in \mathbb{X}$. The two constants q_u and q_d characterizing the supporting hyperplanes are easily calculated as

$$q_u = c^T p + \|H^T c\|_1 \tag{25}$$
$$q_d = c^T p - \|H^T c\|_1 \tag{26}$$

where $\|\cdot\|_1$ is the 1-norm of a vector.

Then, calculating the supporting hyperplane constant q_u and q_d the intersection is empty if and only if

$$q_u < \frac{y(k)}{\sigma} - 1 \quad \text{or} \quad q_d > \frac{y(k)}{\sigma} + 1 \tag{27}$$

This condition of inconsistency was reported in Vicino and Zappa (1996).

5.5 Intersection between a zonotope and a strip

Definition 6. Given a zonotope $\mathbb{Z} = p \oplus H\mathbf{B^m}$ and a strip $F = x : q_a \leq c^T x \leq q_b$, the ***zonotope tight strip*** is obtained by $\mathbb{S} = F \cap F_S$, where F_S is the zonotope support strip defined by c and $\mathbb{Z}$.

According to Alamo et al. (2005), given the zonotope $\mathbb{Z} = p \oplus HB^r$, the tight strip $\mathbb{S} = \{x \in \mathbb{R}^n : |c^T x - d| \leq \sigma\}$ and vector $\alpha \in \mathbb{R}^n$, we have:

$$\mathbb{Z} \cap \mathbb{S} \subseteq \Theta = \widehat{p}(\alpha) \oplus \widehat{H}(\alpha) B^{r+1} \tag{28}$$

where:

$$\widehat{p}(\alpha) = p + \alpha(d - c^T p) \tag{29}$$
$$\widehat{H}(\alpha) = [(I - \alpha c^T)H \;\; \sigma] \tag{30}$$

Then, it is possible to choose the parameter vector α in such a way that a size criterion for the obtained bound is minimized. Here, we use the method based in the Frobenius norm proposed in Alamo et al. (2005) to select the optimal value of α:

$$\alpha^* = \frac{HH^T c}{c^T HH^T c + \sigma^2} \tag{31}$$

5.6 Expansion of the parameter set

The bound on parameter variation can be expressed as $|\theta(k+1) - \theta(k)| < \Lambda$ which in turn can be expressed as

$$\theta(k+1) \in \theta(k) \oplus \Lambda B^n \tag{32}$$

where Λ is a square matrix with the diagonal equal to λ. One of the principal features of zonotopes is that the Minkowski sum of a box and a zonotope is another zonotope. Therefore, if at time k it is known that the parameter belongs to set $\mathbb{X}_k = p \oplus HB^m$ then using Eq. (32) the parameter set at time $k+1$ can be expressed as $\mathbb{X}_{k+1} = p \oplus HB^m \oplus \Lambda B^n = p \oplus [H \; \Lambda] B^{m+n}$.

Notice that in this step the zonotope order increases at each time instant. In order to control the domain complexity, a reduction step is thus implemented. Here we use the method proposed in Combastel (2003) to reduce the zonotope complexity.

Remark. In the time-varying case ($\lambda = \infty$) as the parameters can vary at will within the initial parameter set Θ, the update procedure of step 9 of *Algorithm 2*, consists on resetting $\overline{AFSS}_{k+1}$ equal to the initial parameter set Θ.

6. APPLICATION EXAMPLE

A quadruple-tank process (see Johansson (2000)) is proposed as the application example to further compare the two fault detection tests proposed.

The process inputs are v_1 and v_2 (input voltages to the pumps). The experiments presented in this section just considers the analytical redundancy relation coming from

the first tank assuming that levels h_1, h_3 and voltage v_1 are measured:

$$\frac{d\,h_1}{dt} = -\frac{a_1}{A_1}\sqrt{2gh_1} + \frac{a_3}{A_1}\sqrt{2gh_3} + \frac{\gamma_1 k_1}{A_1}v_1 + e_1 \quad (33)$$

where $A_1 = 28 \quad cm^2$, $k_1 = 3.33 \quad cm^3/Vs$ and $g = 981 \quad cm/s^2$. Parameters a_1 and γ_1 are assumed to belong to the intervals $a_1 \in [0.02, 0.171]$ and $\gamma_1 \in [0.55, 0.85]$. The term e_1 is a bounded random noise with $|e_1| \leq 0.02$. The fault detection algorithm is tested in three different cases of parametric fault scenarios affecting a_1 and γ_1. For all cases the non-faulty system is simulated with parameters equal to $a_1 = a_3 = 0.071 \quad cm^2$, $a_2 = a_4 = 0.057 \quad cm^2$, $\gamma_1 = 0.7$ and $\gamma_2 = 6$.

Equation (33) can be expressed in the form given by Eq. (1), once Euler discretization with sampling time equal to 1 has been applied:

$$h_1(k+1) = h_1(k) - \frac{a_1}{A_1}\sqrt{2gh_1(k)} + \frac{a_3}{A_1}\sqrt{2gh_3(k)} + \frac{\gamma_1 k_1}{A_1}v_1(k) + e_1(k) \quad (34)$$

Note that the results obtained in this section could be improved using the other three equations of the model. Considering that the parameter vector θ is composed of: $\theta = [a_1 \;\; a_3 \;\; \gamma_1]^T$, the regressor vector can be expressed as follows:

$$\varphi_{y_1}(k) = \left[-\frac{\sqrt{2gh_1(k)}}{A_1} \quad \frac{\sqrt{2gh_3(k)}}{A_1} \quad \frac{k_1 v_1(k)}{A_1}\right]^T \quad (35)$$

Taking into account uncertainty intervals associated to a_1 and γ_1 given above, the initial parameter uncertainty set for the fault detection stage is assumed to be:

$$\Theta = \{\theta : \theta = p_0 + H_0\tilde{\theta}, \|\tilde{\theta}\|_\infty \leq 1\}$$

where:
$p_0 = [0.071 \;\; 0.071 \;\; 0.7]^T$, $H_0 = diag\left([0.1 \;\; 0 \;\; 0.15]^T\right)$.

6.1 Time-invariant parameters

Since uncertain parameters are considered time-invariant, then $\lambda = 0$ in Eq. (4). The fault considered is a variation in the parameters a_1 and γ_1 from time instant $k = 5$. This variation of parameters is inside the allowed interval of both parameters, that is $a_{1f} = a_1 + 0.05$ and $\gamma_{1f} = \gamma_1 + 0.1$. Figure 1 shows the fault detection test using the inverse image. The dashed box represents the allowable parameters a_1 and γ_1. The solid line represents the zonotope intersection of the parameters consistent with the first 4 measurement outputs. The dotted line represents the band of parameters consistent with the measurement output for time instant $k = 5$. As this band does not intersect with the zonotope, a fault is indicated. Figure 2 shows the envelopes generated by the direct image fault detection test and the measurement output $[h_1]$ considering the measurement noise. As the measurement output never leaves the envelopes, no fault is indicated. This shows how the inverse image test is able to detect a fault that consists on a non-allowed time variation of the parameters, while the direct image test is unable.

6.2 Time-varying parameters case 1

In this case, uncertain parameters are considered time-varying with: $\lambda = \begin{bmatrix} 0.01 & 0 \\ 0 & 0.03 \end{bmatrix}$, in Eq. (4). The fault considered is a variation in the parameters a_1 and γ_1 from time instant $k = 5$: $a_{1f} = a_1 + 0.03$ and $\gamma_{1f} = \gamma_1 + 0.05$. Even though with this variation, the parameters are inside their uncertainty intervals, it is higher than the allowed value at each time instant given by λ. Figure 3 shows the fault detection test using the inverse image. The dashed box represents the valid interval for parameters a_1 and γ_1. The solid lines represent the zonotope that bounds the parameters consistent with the first 4 measurement outputs. The dotted line represents the band of parameters consistent with the measurement output for time instant $k = 5$. As this band does not intersect with the zonotope, a fault is indicated. Figure 4 shows the envelopes generated by the direct image fault detection test and the measurement output $[h_1]$ considering the measurement noise. As the measurement output never leaves the envelops, no fault is indicated. As in the previous case, this shows how the inverse image test is able to detect a fault that consists on a non-allowed time variation of the parameters, while the direct image test is unable.

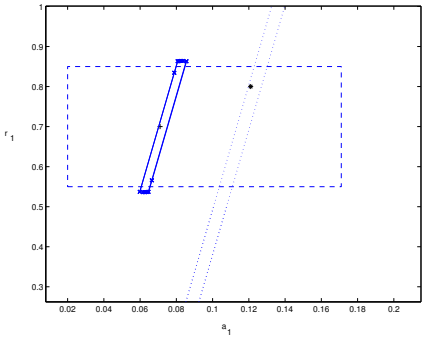

Fig. 1. Inverse image test for time invariant case, a_1 vs. γ_1

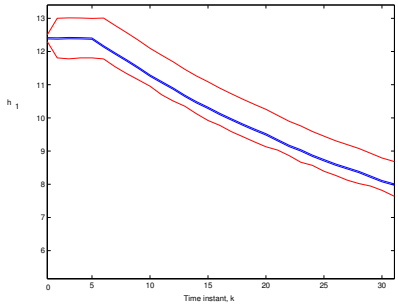

Fig. 2. Direct image test for time invariant case

6.3 Time-varying parameters case 2

In this case, uncertain parameters are considered time-varying with $\lambda = \infty$, in Eq. (4). This means that variation is bounded only by the initial parameter set Θ, varying at will within this set. The fault considered is outside the box of allowed parameters, from time instant $k = 5$, that is $a_{1f} = a_1 + 0.15$. Figure 5 shows the fault detection test using the inverse image. The dashed box represents the allowable parameters region for a_1 and

γ_1. The dotted line represents the band of parameters consistent with the measurement output for time instant $k = 5$. As this band does not intersect with the box of allowed parameters, a fault is indicated. Figure 6 shows the envelopes generated by the direct image fault detection test and the measurement output $[h_1]$ considering the measurement noise. As the measurement output leaves the envelopes from time instant $k = 6$, a fault is indicated. In this case, both methods detect the fault, being not clear the advantage of using the inverse image test.

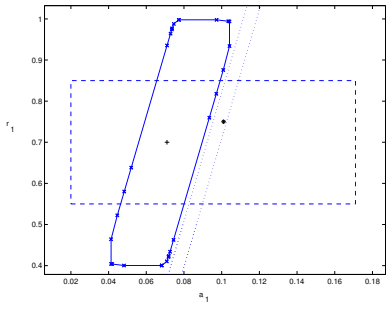

Fig. 3. Inverse image test for time-varying case 1, a_1 vs. γ_1

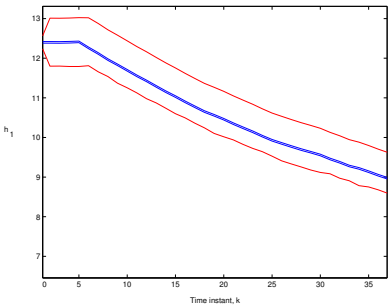

Fig. 4. Direct image test for time-varying case 1

7. CONCLUSIONS

A robust fault detection test based on the inverse image using zonotopes for systems linear in the parameters has been introduced. A general algorithm was presented based on proving that the feasible solution set of parameters for a series of data is empty. Three distinct cases of allowed parameter variance have been considered to compare the inverse test with the traditional interval based fault detection test based on the direct image. Finally, both methods were applied to motivational example and to a simulation model of the known quadruple-tank process, showing the effectiveness of the inverse image fault detection test when considering time varying and invariant parameters. As future work, the method will be extend to the MIMO MA parity equation case.

REFERENCES

O. Adrot and S. Ploix. Fault detection based on set-membership inversion. In *Proceedings of IFAC SAFEPROCESS 2006*, Beijing, China, 2006.

T. Alamo, J.M. Bravo, and E.F. Camacho. Guaranteed state estimation by zonotopes. *Automatica*, 41(6):1035–1043, 2005.

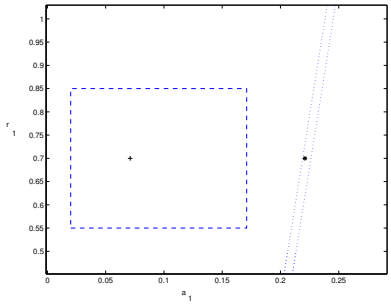

Fig. 5. Inverse image test for time-varying case 2, a_1 vs. γ_1

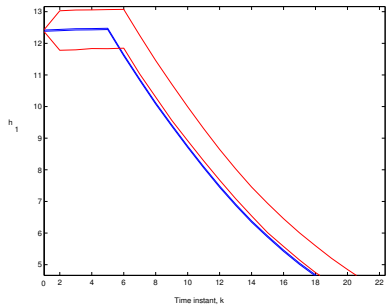

Fig. 6. Direct image test for time-varying case 2

J. Armengol, J. Vehi, L. Trav-Massuys, and M. A. Sainz. Application of multiple sliding time windows to fault detection based on interval models. In *in Proc. 12th Int. Workshop on Principles of Diagnosis (DX-01)*, page 916, Sansicario, Italy, 2001.

J. Chen and R.J. Patton. *Robust Model-Based Fault Diagnosis for Dynamic Systems*. Kluwer Academic Publishers, 1999.

C. Combastel. A state bounding observer based on zonotopes. In *European Control Conference (ECC'03)*, Cambridge, UK, 2003.

I. Fagarasan, S. Ploix, and S. Gentil. Causal fault detection and isolation based on a set-membership approach. *Automatica*, 40:2099–2110, 2004.

L. Jaulin, M. Kieffer, I. Braems, and E. Walter. Guaranteed nonlinear estimation using constraint propagation on sets. *International Journal of Control*, 74(18):1772–1782, 2001.

K.H. Johansson. The quadruple-tank process: A multivariable laboratory with an adjustable zero. *IEEE Transactions on Control Systems Technology*, 8(3):456–465, 2000.

S. Ploix and O. Adrot. Parity relations for linear uncertain dynamic systems. *Automatica*, 42:1553 1562, 2006.

V. Puig, J. Quevedo, T. Escobet, and S. De Las Heras. Robust fault detection approaches using interval models. In *IFAC World Congress (b'00)*, Spain, 2002.

V. Puig, A. Ingimundarson, and S. Tornil. Robust fault detection using inverse images of interval functions. In *Proceedings of IFAC SAFEPROCESS 2006*, Beijing, China, 2006.

A. Vicino and G. Zappa. Sequential approximation of feasible parameter sets for identification with set membership unvertainty. *IEEE Transactions on Automatic Control*, 41:774–785, 1996.